ISSN (Print) 1226-1750
ISSN (Online) 2233-6656
Journal of Magnetics 27(4), 379-387 (2022) https://doi.org/10.4283/JMAG.2022.27.4.379

Electromagnetic Field Analysis of Distributed Winding Permanent Magnet Synchronous Motor Considering Axial Leakage Flux using Two-Dimensional Finite-Element Analysis

Jae-Woo Jung[1]*, Byeong-Hwa Lee[2], and Dong-Gyun Ahn[3]

[1]*Department of Electrical Engineering, Daegu University, Gyeongsan 38453, Republic of Korea*
[2]*Electric Powertrain R&D Center, Korea Automotive Research Institute, Daegu 42704, Republic of Korea*
[3]*Motor Development Department, LG Magna e-Powertrain Korea, Incheon 22744, Republic of Korea*

(Received 10 May 2022, Received in final form 7 October 2022, Accepted 11 October 2022)

This paper proposes a method for the electromagnetic field analysis of permanent magnet synchronous motors (PMSMs) considering the axial leakage flux. To the axial leakage flux while employing two-dimensional (2D) finite-element analysis (FEA), the permeance of the axial leakage path is added into a slot region by increasing the permeability of elements in that region. The increased permeability is calculated based on the permeance relationship of the main magnetic and axial leakage paths, which are calculated using the equivalent magnetic circuit method. The effect of the proposed method is verified by comparing it with the 3-dimensional FEA results. The proposed coupling method uses finite element analysis and is developed from the lumped method proposed in our previous research. The developed method enables the analysis of distributed winding machines, which is not possible with the existing method.

Keywords : axial leakage flux, equivalent magnetic circuit, finite-element analysis, permeability

1. Introduction

Permanent magnet synchronous motors (PMSMs), such as in-wheel systems, are required to have a pancake shape because of the limited installation space [1]. However, the torque of a motor having such a flat shape is affected more by the axial leakage flux than that for a motor having a long axial length. The presence of the axial leakage flux makes it difficult to predict the motor performance using 2-dimensional finite-element analysis (2D FEA). With three-dimensional FEA (3D FEA), the leakage flux can be considered; however, it requires a much greater analysis time. Despite the recent drastic improvement in computational capabilities, 3D FEA remains a burden to designers. Therefore, a suitable approach is required to reflect the axial leakage flux under 2D FEA conditions.

Previous researches have proposed various methods that consider the axial leakage flux. However, these studies had a limitation in that the proposed methods could achieve high analysis reliability only in the no-load state [2-4]. To compensate for this drawback, the authors proposed a method to improve the reliability of the magnetic circuit analysis results under both load and no-load conditions considering the axial leakage flux using only 2D FEA by correcting the previous slot permeability [5, 6]. However, this method was applicable primarily to the concentrated winding and not to the distributed winding model. This is because, in the case of the distributed winding model, the flux path leaks from one tooth across multiple teeth, and therefore it cannot be modeled using the conventional method. In addition, there is a disadvantage in that it takes a long time to set the pre-process as a method of imparting permeability by dividing the air region into finite sections.

This study proposes a novel 2D FEA method that considers the axial leakage flux in a distributed winding model. Unlike the existing method, the proposed method minimizes the time consumed in the pre-process by calculating the permeability coefficient considering the shape of the triangular mesh itself in the finite-element modeling and assigning it to each element. In addition, compared to the concentrated winding model, the main leakage flux path of the distributed winding model has an additional path that crosses multiple teeth in the axial

*Corresponding author: Tel: +82-53-850-6626
Fax: +82-53-850-6619, e-mail: jjw@daegu.ac.kr

direction. In this study, the analysis method applicable to the distributed winding model is addressed by considering the need for an additional magnetic circuit, which has not been reported in previous studies. Moreover, although the analysis of only the distributed winding model is discussed in this paper, the proposed analysis method can also be applied to the analysis of the concentrated winding model. Furthermore, the effect of the proposed method is verified by making comparisons with the 3D FEA results.

2. Magnetic Circuit of Analysis Model

2.1. Prototype for analysis

The prototype is an inserted permanent magnet synchronous motor (IPMSM) that was applied to an integrated starter and generator (ISG) for a hybrid electric vehicle [7]. As shown in Fig. 1 and Table 1, the prototype was designed using six poles and 36 slots with distributed winding. The representative dimension and disassembled sample of the prototype are shown in Fig. 1.

Owing to the proprietary nature of the design, specific dimensions of the analysis model and the maximum torque and current cannot be revealed.

The assembled motor, which is shown in Fig. 1(b), has a long axial length compared with the rotor diameter, so the influence of the axial leakage flux did not significantly affect the current versus torque characteristic. As the motor line-up can be constructed with various capacities

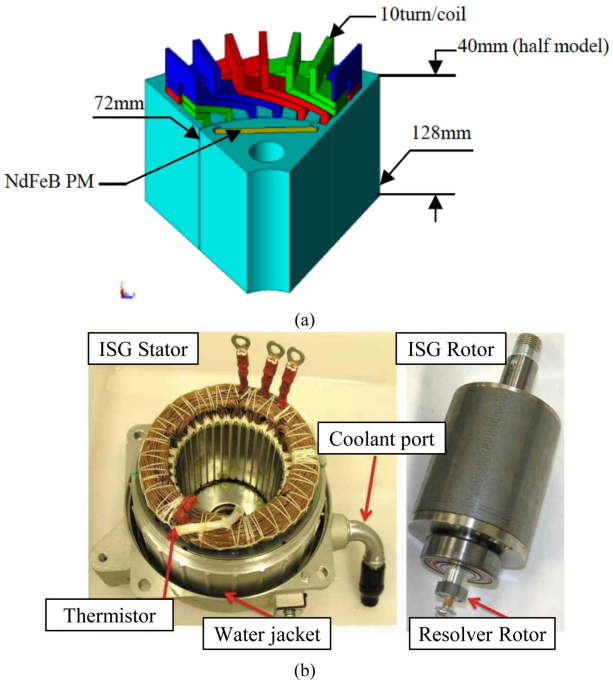

Fig. 1. (Color online) Shape of prototype (a) 1/12 model for FEA, (b) Disassembled sample of prototype [8].

Table 1. Specification of prototype.

Part	Value	Note
Number of pole (ea)	6	-
Number of slot (ea)	36	-
Stator O.D. (mm)	128	-
Rotor O.D. (mm)	72	-
Stack length (mm)	80	Rotor & Stator Core
Winding type	Distributed winding	Coil pitch: 5-slot
DC voltage (V)	210	Battery voltage
Maximum current (A)	125	r.m.s. value
Maximum torque (N·m)	43.2	@ max. current

by varying only the axial length of the manufactured motor, it is necessary to analyze the short axis length of the motor. The characteristics of a motor with a short axial length are influenced by the end leakage magnetic flux; therefore, a suitable analysis method is required to achieve accurate results.

2.2. Magnetic circuit of prototype

To understand the magnetic circuit distribution of the prototype, 3D FEA was performed. In particular, it has been confirmed that the axial leakage magnetic flux near the end turn is distributed according to the current magnitude. The 3D FEA of the prototype was performed using JMAG, which is a commercial FEA software.

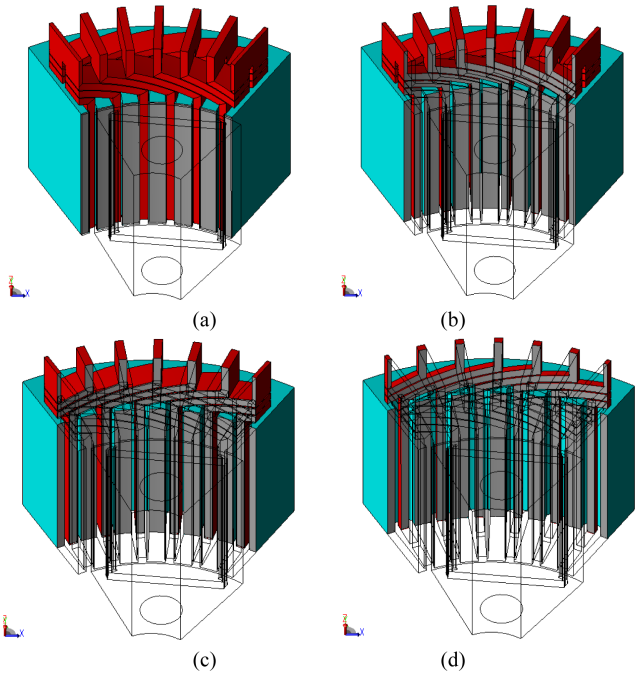

Fig. 2. (Color online) Contour area to confirm the magnetic flux density distribution. (a) 73.8 mm, (b) 83.8 mm, (c) 93.8 mm, and (d) 103.8 mm.

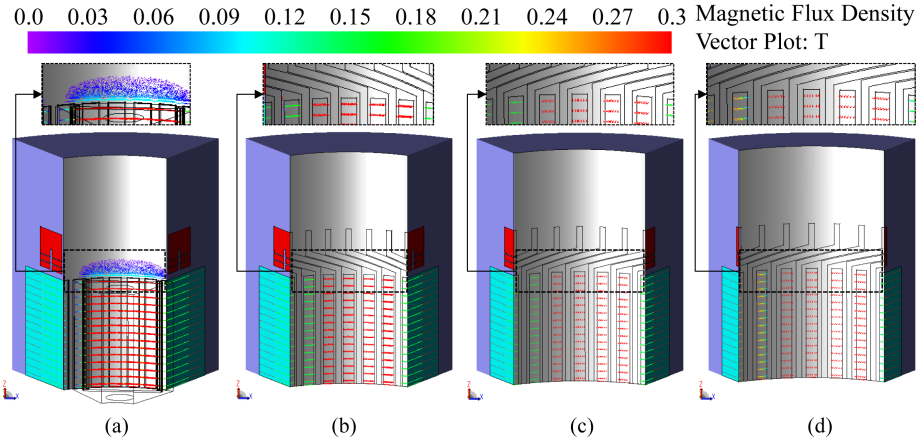

Fig. 3. (Color online) Flux distribution of no-load condition for center diameter of each area. (a) 73.8 mm, (b) 83.8 mm, (c) 93.8 mm, and (d) 103.8 mm.

Figure 2 shows the axial leakage flux distribution under no-load and load conditions. As shown in Fig. 1(b), the prototype was wound into a round wire, but was modeled in a hairpin shape for ease of FEA modeling and analysis, as shown in Fig. 1(a). Because the magnetic flux density distribution of the stator differs in all cases in the radial direction, axial flux leakage along the contour surface was confirmed. Each location of the contour surface is shown in Fig. 2.

Figure 3 shows the axial leakage flux distribution when no current was applied. Considering that the maximum value of the magnetic flux density was 0.3 T, it is evident that the axial leakage magnetic flux was barely visible, except for the contour diameter of 73.8 mm. In the case of a contour surface at 73.8 mm, an axial leakage magnetic flux was observed even under the no-load condition because it was closest to the air-gap. However, its value was less than 0.1 T, which is not sufficiently large to affect the no-load characteristics. Figure 4 shows the axial leakage magnetic flux distribution when the maximum current was applied. As the radius of the contour surface approaches the airgap, the axial leakage magnetic flux increases. In contrast to the leakage magnetic flux distribution observed in previous studies [5] and [6] that focus on the axial leakage magnetic flux of the concentrated winding model, the presence of both leakage magnetic fluxes between adjacent teeth and magnetic circuits leaking through several teeth was confirmed.

3. Leakage Projection Method

This section discusses an analysis method for projecting the axial leakage flux on the 2D plane in a distributed winding model with various leakage paths compared with

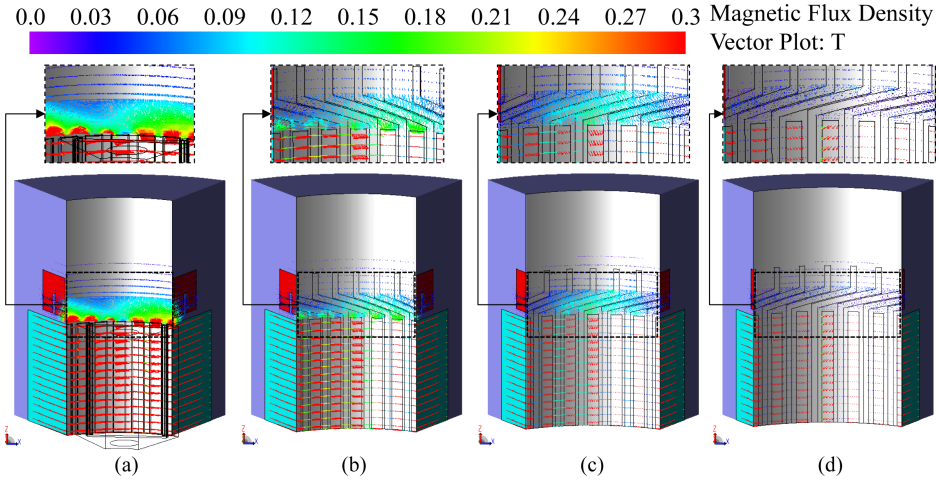

Fig. 4. (Color online) Flux distribution for on-load condition (maximum current condition) for center diameter of each area. (a) 73.8 mm, (b) 83.8 mm, (c) 93.8 mm, and (d) 103.8 mm.

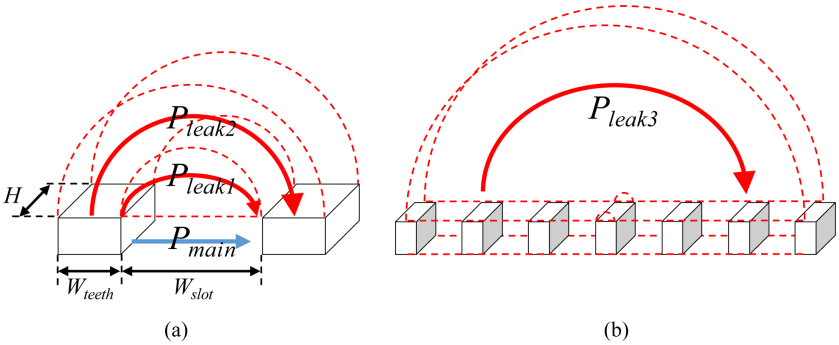

Fig. 5. (Color online) Assumed flux path. (a) Leakage path in slots adjacent to each other, (b) Longest leakage path.

the concentrated winding model. To improve the existing method of projecting the axial leakage magnetic flux onto the 2D plane by dividing the finite number of regions, the axial leakage magnetic flux can be calculated using 2D FEA by modeling each element in FEA. This method is referred to as a leakage projection method.

3.1. Computation method for projecting the axial leakage magnetic flux on the 2D plane

Figures 3 and 4 show the axial leakage magnetic flux path that reflects the core characteristics for a distributed winding with a closely spaced tooth and slot spacing, and are calculated using 3D FEA. The axial leakage magnetic flux distribution resulting from the 3D FEA was simplified as shown in Fig. 5, and it was applied to the permeance calculation. The permeance P_{main} represents the main leakage path, and the permeance of the axial leakage paths were P_{leak1}, P_{leak2}, and P_{leak3}. While P_{leak3} was not reflected in the lumped winding model, it should be considered in the distributed winding model. The permeance with the longest leakage path, P_{leak3}, spanned six slots, as one pole pitch is equal to six slot pitches. Although it is a five-slot pitch winding, the leakage flux must be considered with the six-slot pitch equal to the pole pitch. All the permeance equations of Fig. 5 are given below:

$$P_{main} = \mu_0 \left(hL_{stk} / W_{slot} \right) \tag{1}$$

$$P_{leak1} = 0.264 \mu_0 h \tag{2}$$

$$P_{leak2} = \mu_0 \frac{h}{\pi} \ln \left(\frac{W}{W_{slot}} \right) \tag{3}$$

$$P_{leak3} = \mu_0 \frac{h}{\pi} \ln \left(\frac{6W}{W_{slot}} \right) \tag{4}$$

$$\begin{aligned} P_{Total} &= P_{main} + 2P_{leak1} + 2P_{leak2} + 2N_p P_{leak3} \\ &= \mu_{rf\_slot} \cdot P_{main} \end{aligned} \tag{5}$$

$$\mu_{rf\_slot} = P_{Total} / P_{main} \tag{6}$$

where L_{stk} is the stack length of the magnetic core, N_p is the number of slots per pole, and μ_{rf_slot} is the relative permeance factor of each element derived by the permeance of the main leakage to the total permeance. Because the variables W and W_{slot} change from the origin to the radius r, it is necessary to calculate W and W_{slot} for each element. Equations (7) and (8) respectively represent W and W_{slot} at the center of each element, and the results for the prototype are shown in Fig. 6(a).

$$W = 2r \times \tan(\pi / N_S) \tag{7}$$

$$W_{\text{slot}} = W - W_{\text{teeth}} \tag{8}$$

where N_S is the number of slots. In the case of the prototype, N_S was 36 and the teeth width, W_{teeth}, was 3.9 mm. By applying μ_{rf_slot} to all the elements in the slot region and performing FEA, the axial leakage flux can be reflected in the 2D FEA. In this case, the permeability of each element should be set to that of an anisotropic material to show that the axial leakage magnetic flux flows vertically from the tooth to a neighboring tooth [9]. The permeability distribution in the radial and tangential directions inside the slot is therefore as shown in Fig. 6(b).

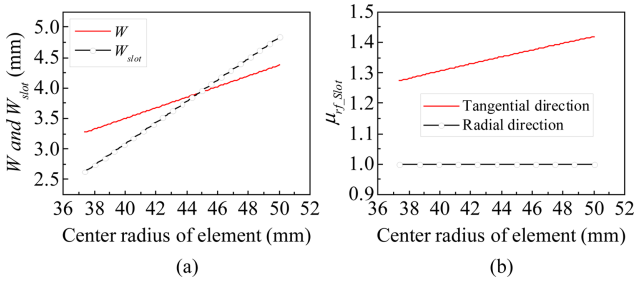

Fig. 6. (Color online) W, W_{slot}, and μ_{rf_slot} according to the center radius of the element. (a) W and W_{slot}, (b) μ_{rf_slot}.

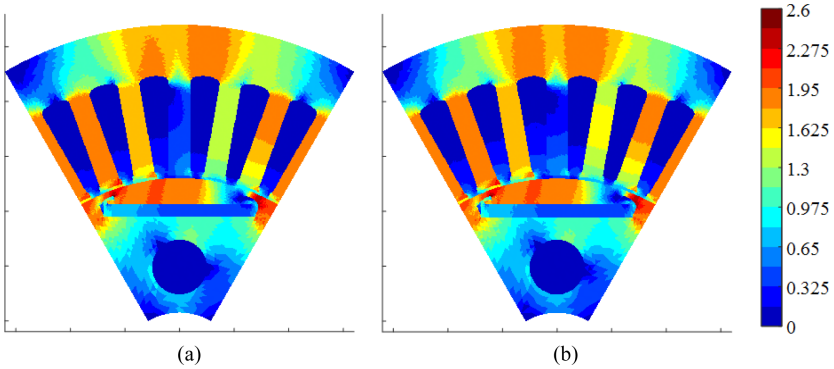

Fig. 7. (Color online) Comparison of flux density distribution (load condition: line current of 124 A and 45° current phase angle). (a) Conventional 2D FEA, (b) Proposed 2D FEA.

3.2. Effect of proposed method - Comparison of magnetic flux density distribution

The magnetic flux density distributions obtained using both the proposed and conventional methods were compared. As shown in Fig. 7, the magnetic flux density distributions obtained by the two methods were different. In particular, the stator yoke was markedly different, and certain changes were observed in the teeth. As shown in Fig. 8, the flux density vector magnitude in the slot region was different owing to the influence of the correction factor μ_{rf_slot}, which was assigned to every element of the slot region. Therefore, it can be concluded that the variation of the flux density distribution of the core observed in Fig. 7 is due to the increase in the slot leakage.

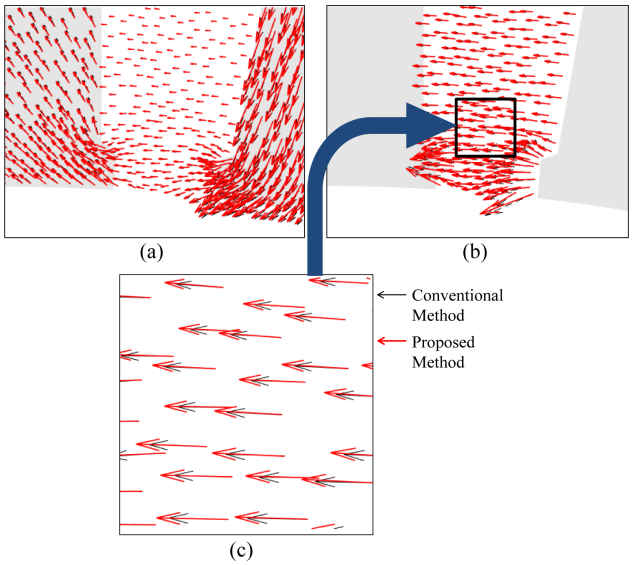

Fig. 8. (Color online) Vector plot of magnetic flux density around stator teeth and slot region (load condition: line current of 124 A and 45° current phase angle). (a) Vector plot for teeth and slot, (b) Vector plot for only slot region, (c) Magnified view of slot region: comparison of vector plot.

4. Verification

Based on the results of the 2D FEA proposed in this study, the ISG model was analyzed for each axial length. To verify the improvement effect of the proposed method, it was compared with the analysis results obtained using both 3D FEA and conventional 2D FEA. Various characteristics, such as the torque for each axial length of the analysis model, the induced electromotive force waveform under specific load conditions, namely *d*- and *q*-axis inductance, and the efficiency were compared.

4.1. No-load induced voltage obtained using axial length

First, the no-load induced voltage, which is one of the most important characteristics of the motor, was calculated and compared according to analysis method and axial length. As shown in Fig. 9, the difference according to the analysis method was very small (the error of the proposed 2D FEA compared to that of the 3D FEA in the axial length 20-mm model was 2.9 %) in all models considering the length in the axial direction. This can be attributed to the small amount of leakage magnetic flux in the axial direction under the no-load condition.

4.2. Torque characteristics obtained using axial length

As the axial length decreases, the influence of the leakage magnetic flux significantly affects the torque value. Therefore, a torque analysis was performed for each axial length, and the difference between the proposed and conventional methods was determined. The reference model with which the torque values per axial length were compared had an axial length of 80 mm. Figures 10(a) and (b) show the torque analysis results under the maximum and rated load conditions, respectively. Figures 11 and 12 respectively show the torque waveforms and values of the average torque for each length in the axial direction

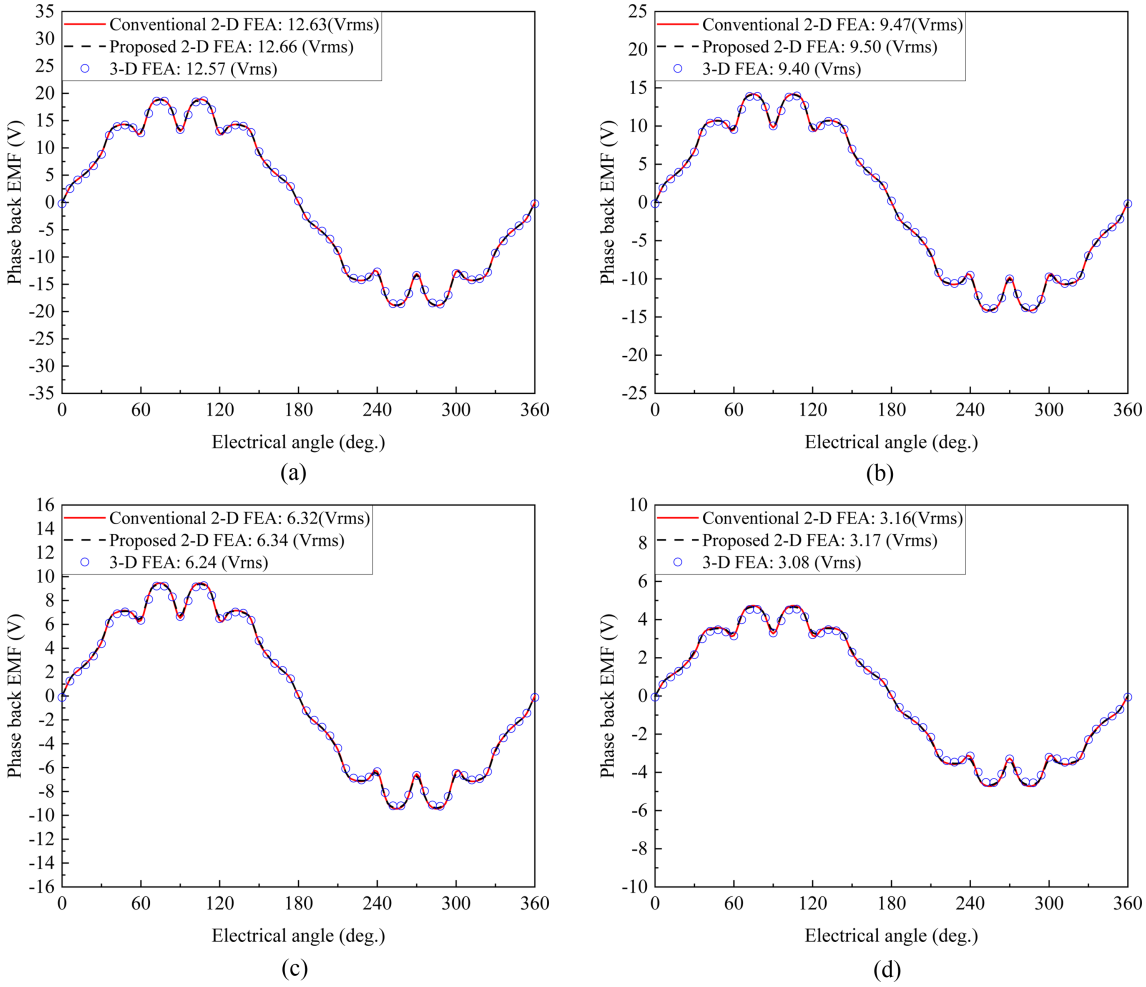

Fig. 9. (Color online) Comparison of no-load induced voltage by axial length. (a) Stack length 80 mm, (b) Stack length 60 mm, (c) Stack length 40 mm, and (d) Stack length 20 mm.

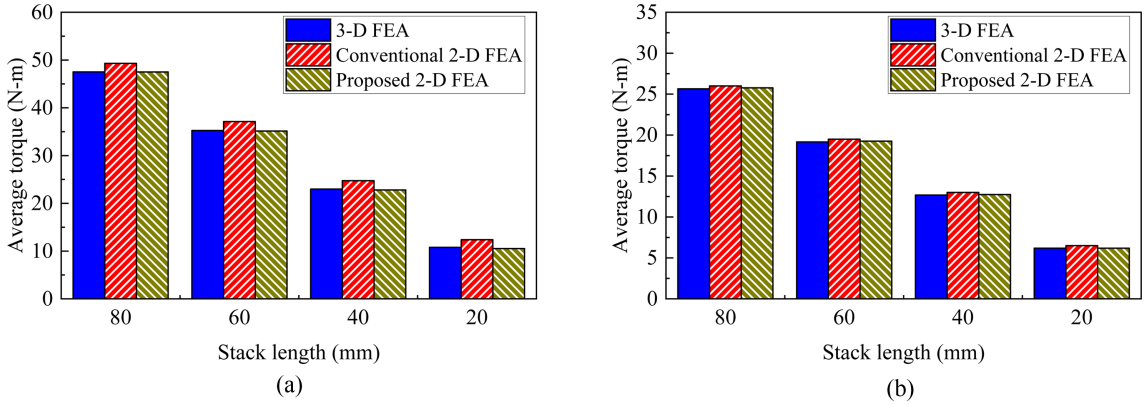

Fig. 10. (Color online) Calculated torque values according to the stack length of the core. (a) RMS value of 124 A and 45° current angle, (b) RMS of 60 A and 45 degree current angle.

according to the analysis method shown in Fig. 10. Each graph in Figs. 10 to 12 shows a different torque according to the analysis method depending on the axial stack length. It was concluded that the error between the 3D FEA and the conventional 2D FEA results increased because the axial leakage magnetic flux increased with a high applied current. In addition, the smaller the axial length, the larger is the ratio of the axial leakage fluxes to

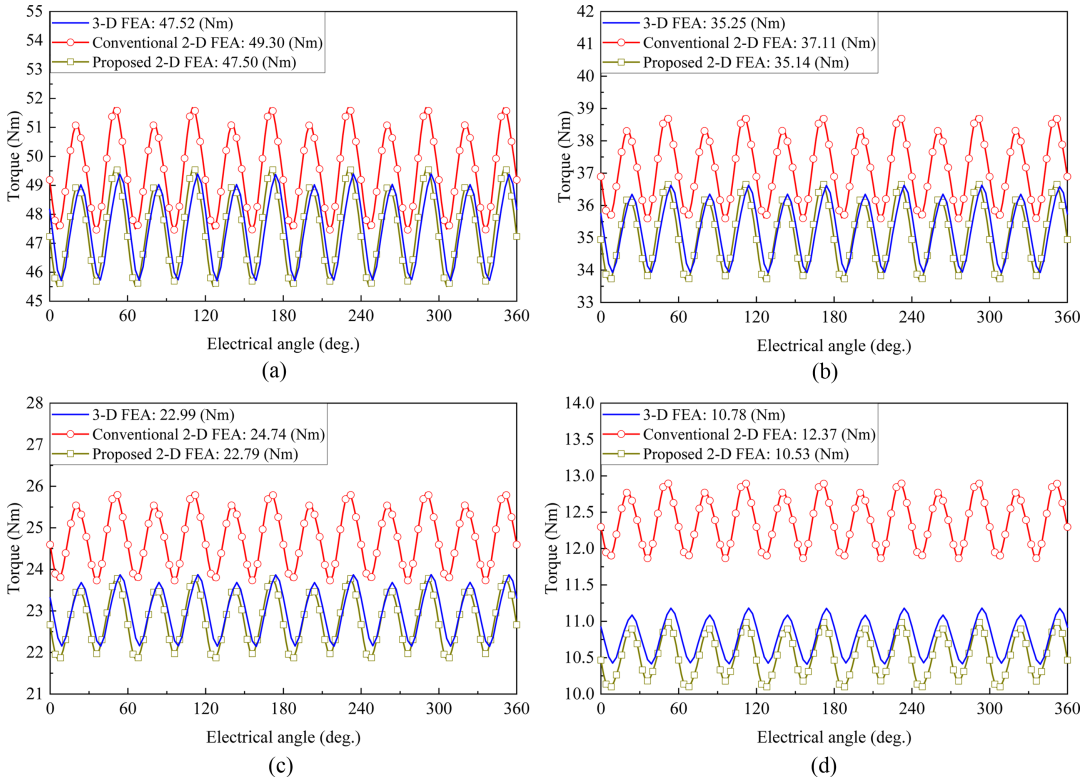

Fig. 11. (Color online) Comparison of torque waveform and values according to the stack length of the core. @RMS value of 125 A and 45° current angle (a) Stack length 80 mm, (b) Stack length 60 mm, (c) Stack length 40 mm, and (d) Stack length 20 mm.

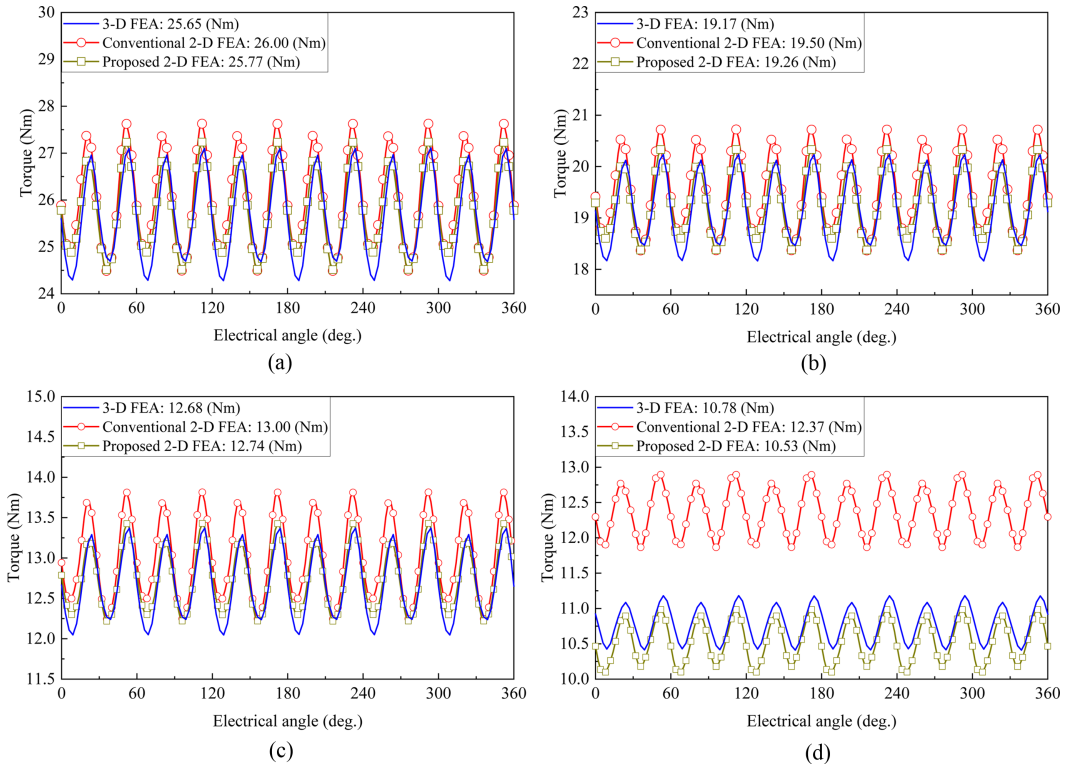

Fig. 12. (Color online) Comparison of torque waveform and values according to the stack length of the core. @ RMS value of 60 A and 45° current angle, (a) Stack length 80 mm, (b) Stack length 60 mm, (c) Stack length 40 mm, (d) Stack length 20 mm.

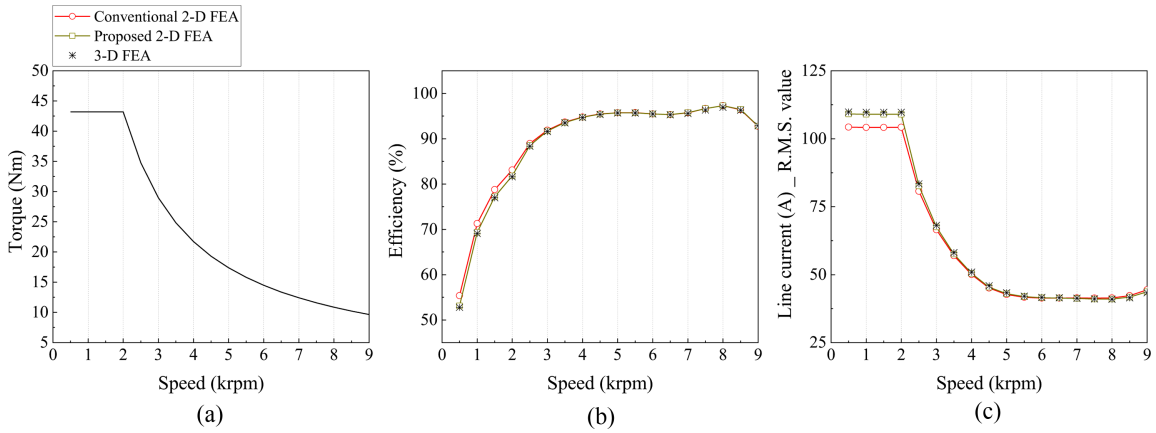

Fig. 13. (Color online) Comparison of characteristic curves according to the analysis method of a model with an axial length of 80 mm.

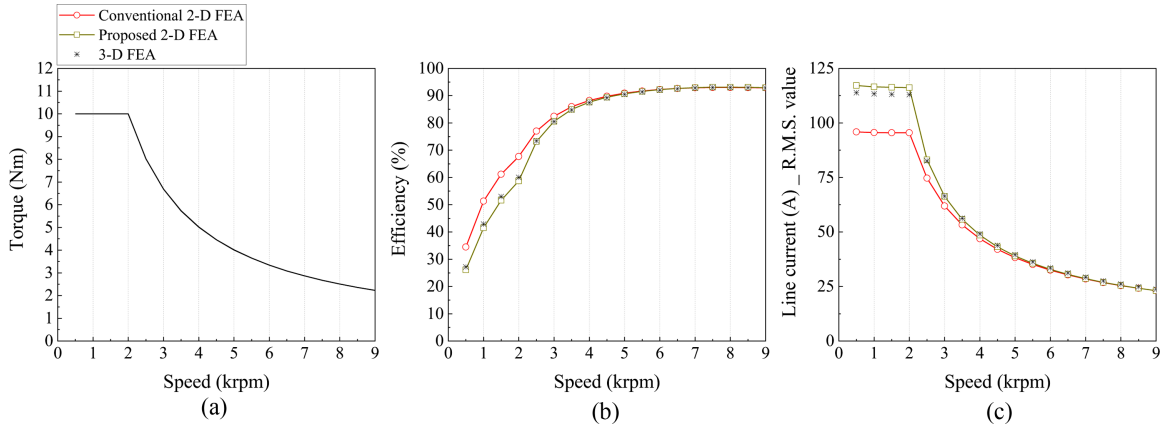

Fig. 14. (Color online) Comparison of characteristic curves according to the analysis method of a model with an axial length of 20 mm.

the total magnetic flux. Thus, the difference between the 3D FEA and the conventional 2D FEA results increases. However, when using the proposed method, the analysis results were found to be similar to the results of the 3D FEA irrespective of the magnitude of the applied current and the axial stack length.

4.3. Comparison of characteristic curves using analysis method

It was confirmed that the proposed 2D FEA exhibited an accuracy similar to that of the 3D FEA based on the comparison of the torque calculation results for each axial length previously presented. We analyzed the overall load characteristics of the analysis model by using each type of analysis method (conventional method, proposed method, 3D FEA). Comparisons were performed according to the axial length of the analysis model and the analysis method. We derived the performance curve of the analysis model for each analysis method under limited input power conditions (maximum DC voltage and line current limit). To analyze the performance of the analysis model, the inductance profile for each current and current phase angle was calculated and then applied to the *d*- and *q*-axis equivalent circuit analysis [10].

The efficiency and line current calculated using the *d*- and *q*-axis equivalent circuit analysis were compared for each type of analysis method. The analysis was performed on the model that was least affected by the leakage magnetic flux in the axial direction (axial length of the 80 mm model) and the model that was most affected by the influence of the leakage flux in the axial direction (axial length of the 20 mm model). Figure 13 shows the analysis result obtained for the axial length of the 80 mm model. With respect to the efficiency of the same torque-speed curve, according to the analysis method, the difference was not large. However, it was slightly lower than the result calculated using the conventional method or the remaining values. The efficiency and line current of 3D

FEA and the proposed method were almost identical. In the constant-torque region, the line current difference between the conventional method and 3D FEA was 5 %. Figure 14 shows the characteristic results obtained for each analysis method for an analysis model with an axial length of 20 mm. The difference in the calculation results for each analysis method was similar to the above-described 80-mm model. Further, the calculated line current in the constant-torque region was approximately 2.7 % lower than the value calculated using the proposed method, compared with the result calculated using 3D FEA. However, the current obtained using the conventional method exhibited an error that was 8.2 % lower than the result obtained by 3D FEA. This is because the influence of the leakage magnetic flux in the axial direction increases as the axial length of the core decreases.

5. Conclusion

This study proposed a finite-element analysis method for an IPMSM with six poles and 36 slots in distributed winding. The leakage projection method was introduced to reflect the axial leakage flux that is generated when the magnetic saturation of the tooth region is high, even though it is a 2D analysis. In contrast to the method proposed in the previous research, the accuracy and convenience of the analysis can be improved by applying the permeability correction factor, μ_{rf_slot}, to each element automatically. In this study, this analysis method was verified for the distributed winding model. However, this analysis method can be used in the case of the concentrated winding model by eliminating the leakage path 3, P_{leak3}, in the axial leakage path.

The analysis model used to verify the proposed analysis method was analyzed while reducing the axial length by 20 mm, from an axial length of 80 mm. It was confirmed that the proposed analysis method reflects the effect of the leakage flux in the axial direction under the rated load condition, and it was particularly effective as the axial length of the analysis model decreased. It was confirmed that the proposed analysis method at the maximum rated load reflected the leakage flux in the axial direction and output the torque value. Further, under the maximum rated condition, a difference of as small as 3.6 % (length in the axial direction of 80 mm) and as high as 14.8 % (length in the axial direction of 20 mm) was confirmed.

As shown in the analysis results, the proposed method was more effective in the case of the model with a short axial length and a high saturation of magnetic flux density under full-load conditions. Therefore, it is believed that it will be suitable in the case designing a line-up models with various output power using the same core shape.

Acknowledgment

This work was supported by the National Research Foundation of Korea (NRF) grant funded by the Korea government (MSIP; Ministry of Science, ICT & Future Planning) (NRF-2021R1G1A1095642).

References

[1] K. M. Rahman, N. R. Patel, T. G. Ward, J. M. Nagashima, F. Caricchi, and F. Crescimbini, IEEE Trans. Ind. Appl. **42**, 1185 (2006).
[2] S. G. Lee, J. Lee, and W. H. Kim, IEEE Trans. Magn. **53**, 8201404 (2017).
[3] S. G. Lee, J. N. Bae, and W. H. Kim, IEEE Trans. Magn. **28**, 5200705 (2018).
[4] Yu Chen, Z. Q. Zhu, and David Howe, IEEE Trans. Ind. Appl. **44**, 1701 (2008).
[5] J. W. Jung, H. I. Park, J. P. Hong, and B. H. Lee, IEEE Trans. Magn. **53**, 8208104 (2017).
[6] J. W. Jung, M. S. Lim, J. P. Hong, and B. H. Lee, IEEE Trans. Magn. **54**, 8200904 (2018).
[7] J. W. Jung, S. H. Lee, G. H. Lee, J. P. Hong, D. H. Lee, and K. N. Kim, IEEE Trans. Magn. **46**, 2454 (2010).
[8] M. Olszewski, Oak Ridge National Laboratory Annual Progress Report for the Power Electronics and Electric Machinery Program, Oak Ridge National Laboratory 110 (2011).
[9] Jin Liu and G. H. Shirkoohi, IEEE Trans. Magn. **29**, 2458 (1993).
[10] B. H. Lee, S. O. Kwon, T. Sun, J. P. Hong, G. H. Lee, and J. Hur, IEEE Trans. Magn. **47**, 1066 (2011).